Anisotropic high-field terahertz response of free-standing carbon nanotubes

Byounghwak Lee,[1] Ali Mousavian,[1] Michael J. Paul,[1] Zachary J. Thompson,[1] Andrew D. Stickel,[1] Dalton R. McCuen,[1] Eui Yun Jang,[2] Yong Hyup Kim,[2] Jisoo Kyoung,[3] Dai-Sik Kim,[3] and Yun-Shik Lee[1,a)]
[1]*Department of Physics, Oregon State University, Corvallis, Oregon 97331-6507, USA*
[2]*School of Mechanical and Aerospace Engineering, Seoul National University, Seoul 151-744, South Korea*
[3]*Department of Physics and Astronomy, Seoul National University, Seoul 151-747, South Korea*

(Received 27 April 2016; accepted 6 June 2016; published online 17 June 2016)

We demonstrate that unidirectionally aligned, free-standing multi-walled carbon nanotubes (CNTs) exhibit highly anisotropic linear and nonlinear terahertz (THz) responses. For the polarization parallel to the CNT axis, strong THz pulses induce nonlinear absorption in the quasi-one-dimensional conducting media, while no nonlinear effect is observed in the perpendicular polarization configuration. Time-resolved measurements of transmitted THz pulses and a theoretical analysis of the data reveal that intense THz fields enhance permittivity in carbon nanotubes by generating charge carriers. *Published by AIP Publishing.* [http://dx.doi.org/10.1063/1.4954222]

Electron dynamics in carbon nanotubes (CNTs) typically fall in the terahertz (THz) frequency region.[1–4] The high responsivity of CNTs to THz electromagnetic waves creates great potential for a wide range of applications, including ultrafast nanoelectronics,[5–7] THz sources[8,9] and detectors,[10–12] and THz optical elements.[13,14] CNT based THz polarizers, in particular, exploit the highly anisotropic THz response of quasi-one-dimensional CNTs.[15–17] These applications are based on the linear THz response of CNTs involving low-field electron dynamics. High-field electron dynamics become important when CNT devices shrink to nanometer dimensions, where operating frequencies are in the THz range and internal electric fields exceed 100 kV/m. It is, however, rarely studied how electrons in CNTs behave in the presence of strong THz fields. The only experimental study reported so far is that strong THz fields generate excitons in semiconductor single-walled CNTs (SWNTs).[18]

In this paper, we present an experimental study to investigate the high-field THz response of free-standing multi-walled CNTs (MWNTs). We demonstrate that unidirectionally aligned free-standing MWNTs form a quasi-one-dimensional metallic structure and exhibit highly anisotropic linear and nonlinear THz responses. In particular, strong THz pulses induce nonlinear absorption in MWNTs. This is unusual because strong THz pulses generally induce transparency in a conducting medium.[19,20] The THz induced absorption indicates that intense THz fields enhance the permittivity of the MWNTs.

We performed a nonlinear THz transmission spectroscopy of free-standing MWNTs. A forest of MWNTs (diameter, 10 nm; averaging 9 walls per tube) was synthesized by catalytic chemical vapor deposition and CNT sheets were drawn from the forest.[21,22] We fabricated the samples by depositing the CNT sheets multiple times on a U-shaped polyethylene (PE) reel (thickness, 125 μm).[16] An SEM image of the sample is shown in Fig. 1(a). Areal density of the CNT sheets (thickness, 50 nm) is proportional to the deposition number N_w on the PE reel. We tested four free-standing MWNT samples of $N_w = 2$, 5, 10, and 20.

We generate strong THz pulses (central frequency, 0.9 THz; bandwidth, 1 THz; THz field amplitude, 1 MV/cm) via optical rectification of femtosecond laser pulses (pulse energy, 1 mJ; pulse duration, 100 fs; repetition rate, 1 kHz) with titled pulse front for phase matching between optical and THz pulses in $LiNbO_3$.[19,20,23] THz pulses are focused onto a sample with parabolic mirrors (beam diameter, 370 μm at focus). We detect THz pulses using a liquid-He cooled Si:Bolometer and electro-optic (EO) sampling with a 1-mm ZnTe crystal.

THz response of CNT is highly anisotropic due to the quasi-1D structure; THz polarization parallel to the CNT axis elicits a significantly stronger response compared to the perpendicular case.

We first present THz transmission for the THz polarization perpendicular to the CNT axis measured by the Si:Bolometer (Fig. 1). The raster scanning image of THz transmission of the $N_w = 10$ sample in Fig. 1(b) is spatially homogeneous, indicating that CNTs are uniformly distributed over the large area of the sample. Figure 1(c) shows the THz transmission of the CNT samples (N_w = 2, 5, 10, and 20) as a function of the peak-field amplitude of incident THz pulses. The transmission is flat in the wide range of THz field strength and no sample exhibits nonlinear THz responses. Nonlinear THz response is negligible for the perpendicular polarization configuration because the electron motion is confined to the small dimensions in the radial direction (< 10 nm). The inset in Fig. 1(c) shows THz transmission versus deposition number N_w. The data fits well with an exponential decay, suggesting that the deposition number is proportional to the CNT areal density. The fit gives rise to the perpendicular absorption coefficient, $\alpha_\perp = 0.024$ per deposition.

When the THz polarization is aligned parallel to the CNT axis, THz response of the CNT samples is significantly stronger than that of the perpendicular configuration. (The parallel absorption coefficient $\alpha_\parallel$ is 0.47 per deposition. Transmission

a)Electronic mail: leeys@physics.oregonstate.edu

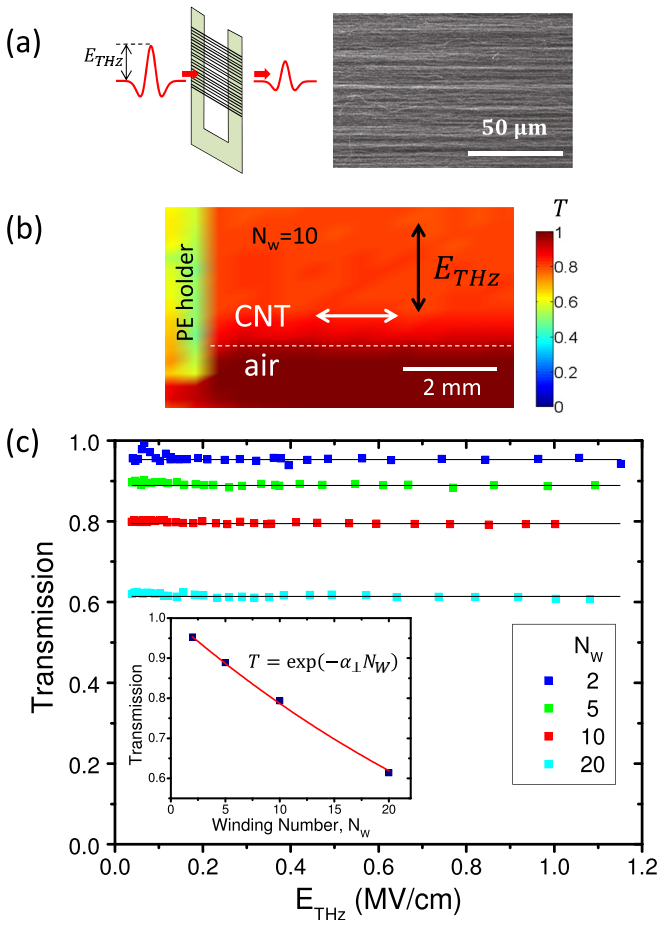

FIG. 1. THz transmission for THz polarization perpendicular to CNT axis measured by a Si:Bolometer. (a) SEM image of the $N_w = 20$ CNT sample. (b) Raster scanning THz transmission image of the $N_w = 10$ CNT sample. The spatially averaged transmission is 0.79. (c) Transmission vs. THz field strength for N_w = 2, 5, 10, and 20. The black lines indicate linear fits. The inset shows transmission vs. deposit number N_w. The red line is an exponential fit, producing the perpendicular absorption coefficient, $\alpha_\perp = 0.024$ per layer.

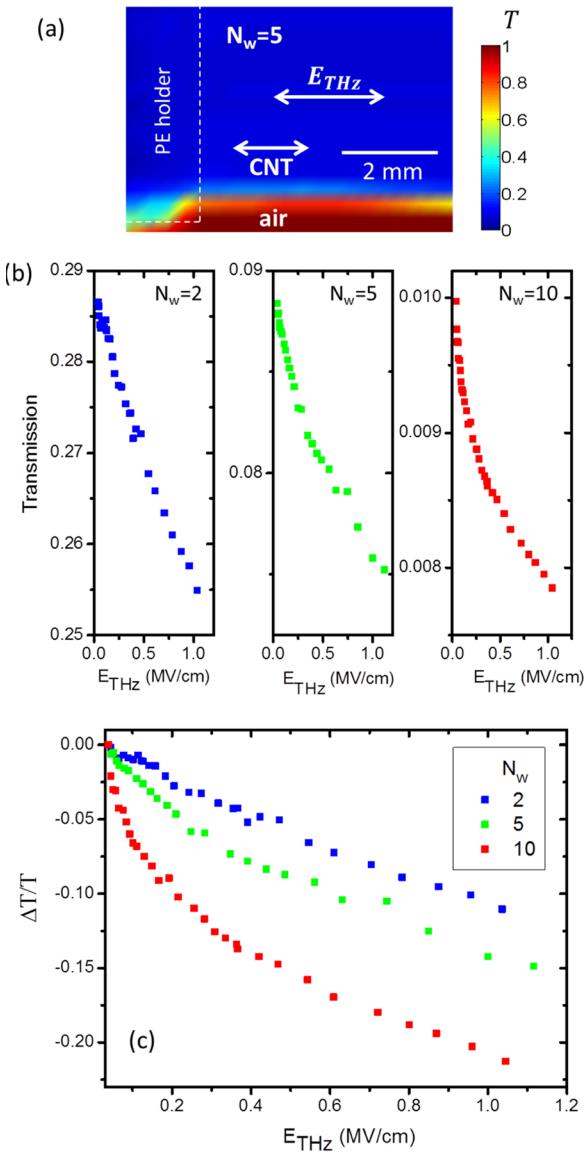

FIG. 2. THz transmission for THz polarization parallel to CNT axis measured by a Si:Bolometer. (a) Raster scanning image of THz transmission of the $N_W = 5$ CNT sample. The spatially averaged transmission is 0.088. (b) Transmission and (c) normalized differential transmission vs. THz field strength for N_W = 2, 5, and 10.

through the $N_w = 20$ sample is too low to acquire meaningful data). The spatially uniform transmission of the $N_w = 5$ sample shown in Fig. 2(a) is $T_\parallel = 0.088$, which is significantly lower than $T_\perp = 0.89$ of the perpendicular configuration. More importantly, the THz transmission of the parallel configuration exhibits strong nonlinear effects. Figure 2(b) shows that the transmission decreases as THz field strength increases, demonstrating that intense THz fields induce nonlinear absorption in the MWNT samples. The nonlinear effects are strong: the transmission change exceeds 10% for $N_w = 2$ and 20% for $N_w = 10$. Figure 2(c) shows that normalized differential transmission ($\Delta T/T$) exhibits a larger change for higher nanotube density.

For a better understanding of the THz induced nonlinear effects, we carry out THz time-domain spectroscopy of the MWNT samples for the parallel polarization configuration. Figure 3 shows the waveforms and amplitude spectra of THz pulses transmitted through the samples at three different THz peak field strengths, E_{THz} = 0.2, 0.5, and 1.2 MV/cm. Transmitted THz waveforms exhibit not only amplitude reduction but also a phase shift as the deposition number and the THz field strength increase (Figs. 3(a)–3(c)). The amplitude spectra in Figs. 3(d)–3(f) show that the THz transmission gradually decreases as the frequency increases.

We obtain the complex refractive index of the MWNT samples analyzing the amplitude and phase spectra of the transmitted THz pulses. The Fresnel transmission coefficient of a layer of thickness d is expressed as a function of frequency,

$$t(\omega) = \frac{4\tilde{n}}{(1+\tilde{n})^2 e^{-i\omega\tilde{n}d/c} - (1-\tilde{n})^2 e^{i\omega\tilde{n}d/c}}, \qquad (1)$$

where $\tilde{n}(\omega) = n_R(\omega) + in_I(\omega)$ is the frequency-dependent complex refractive index of MWNTs. We extract $n_R(\omega)$ and $n_I(\omega)$ using an optimization protocol.[24] For the complex transmission coefficient written as $t(\omega) = \rho \exp(-i\Phi)$, we define the deviation of the theory from the experiment as an elliptic paraboloid,

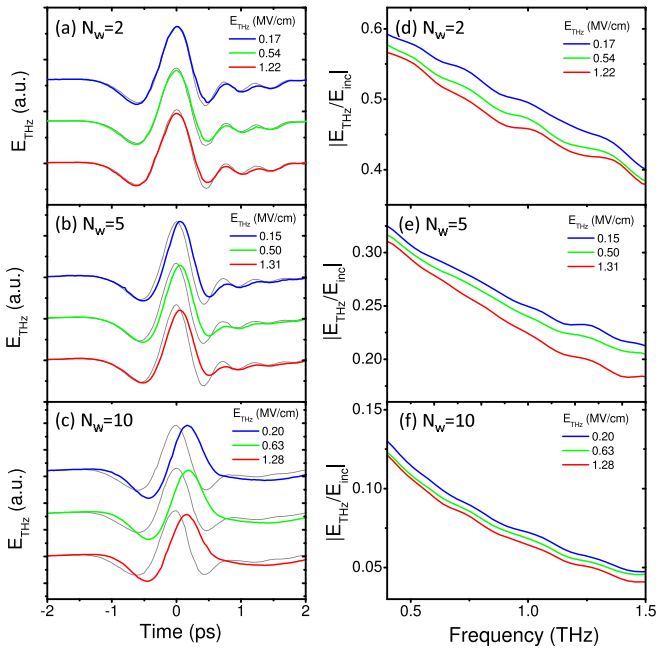

FIG. 3. Waveforms of THz pulses transmitted through (a) $N_w = 2$, (a) $N_w = 5$, and (c) $N_w = 10$ samples for three THz peak field strengths, $E_{THz} \approx 0.2$, 0.5, and 1.2 MV/cm. The gray lines present the incident waveforms normalized to the transmitted waveform of the lowest field strength at $E_{THz} \approx 0.2$ MV/cm. Corresponding amplitude spectra are shown in (d) $N_w = 2$, (e) $N_w = 5$, and (f) $N_w = 10$.

$$\Delta = \delta\rho^2 + \delta\Phi^2, \tag{2}$$

where

$$\delta\rho = \ln(\rho_{\text{theory}}) - \ln(\rho_{\text{exp}}) \tag{3}$$

and

$$\delta\Phi = \arctan(\Phi_{\text{theory}}) - \arctan(\Phi_{\text{exp}}). \tag{4}$$

Using Taylor approximation and Hessian matrix, we solve the elliptic paraboloid equation $\Delta(n_R, n_I) = 0$ and determine the complex relative permittivity, $\varepsilon_r(\omega) = \tilde{n}(\omega)^2$.

Figure 4 shows the spectra of the real and imaginary parts of the relative permittivity of $N_w = 2$, 5, and 10 samples for three THz peak field strengths, $E_{THz} \approx 0.2$ (blue), 0.5 (green), and 1.2 (red) MV/cm. We fit the results to the permittivity of a conducting medium based on Drude model

$$\varepsilon_r(\omega) = \varepsilon_b - \frac{\sigma_0\tau}{\varepsilon_0} + i\frac{\sigma_0}{\varepsilon_0\omega}, \tag{5}$$

where ε_b is the contribution from bound electrons, τ is the scattering time ($\tau \ll \omega^{-1}$), and σ_0 is the DC conductivity of MWNTs. The fitting parameters are the real part of the relative permittivity Re $\{\varepsilon_r\}$, the imaginary part of the bound electron contribution, Im $\{\varepsilon_b\}$, and the DC conductivity σ_0. The fitting curves (solid gray lines in Fig. 4) agree well with the experimental results. The real part of permittivity is spectrally flat and negative, while the imaginary part shows a pattern inversely proportional to ω, corresponding to free-carrier contribution. The large background of the imaginary permittivity suggests that the response of electrons in a shallow trap states is substantial. The permittivities of the MWNT samples are enhanced to a large extent by the strong THz pulses, showing that the intense fields activate strongly nonlinear electron dynamics.

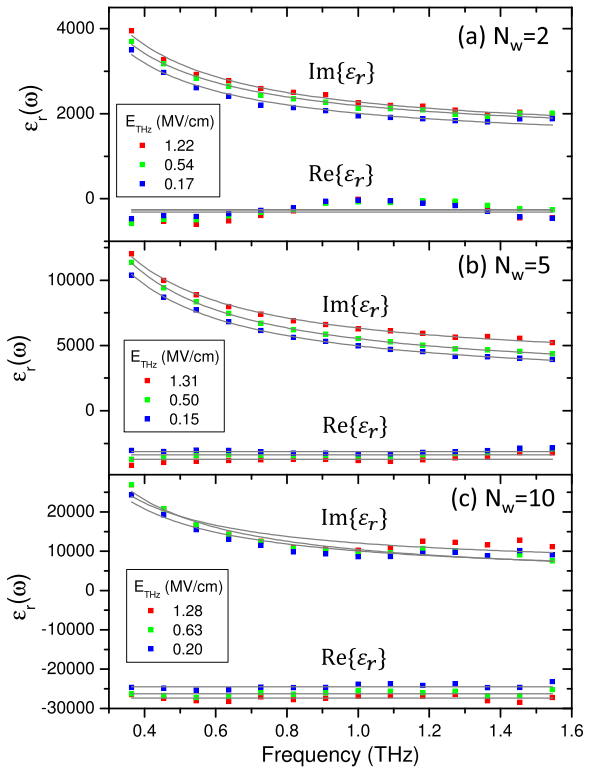

FIG. 4. Relative permittivity of MWNTs: Experimental data (solid squares) and Drude fitting curves (gray lines) of relative permittivity spectra of (a) $N_w = 2$, (c) $N_w = 5$, and (c) $N_w = 10$ samples for three THz peak field strengths, $E_{THz} \approx 0.2$, 0.5, and 1.2 MV/cm.

Figure 5 shows the fitting parameters as a function of THz field strength. The fitting results indicate that the field enhancement of permittivity involves intricate processes. The field induced changes in the parameters depend on the CNT density. This means that the high-field electron dynamics is affected by inter-tube Coulomb interactions, especially in the high density CNT samples of $N_w = 5$ and 10. The magnitudes of Re $\{\varepsilon_r\}$ and Im $\{\varepsilon_b\}$ show the general tendency, increasing as the field strength goes up (Figs. 5(a) and 5(b)). The field dependent conductivity shown in Fig. 5(c) exhibits different features for the different samples. A field induced change in conductivity is caused by two competing processes. In general, intense THz fields reduce conductivity of metallic media by increasing electron temperature and consequently lowering the scattering time.[19,20] On the other hand, conductivity goes up if intense THz fields increase carrier density by generating carriers (probable mechanisms are carrier multiplication by impact ionization[25–27] and field-induced interband tunneling[4,18,23]). The conductivity of the low density CNT sample ($N_w = 2$) increases as the field strength increases, where the effect of the carrier generation dominates that of the scattering time reduction. In the high density CNT samples of $N_w = 5$ and 10, the reduction of the conductivity at the high field strength suggests that the scattering rate becomes much higher than the carrier generation rate.

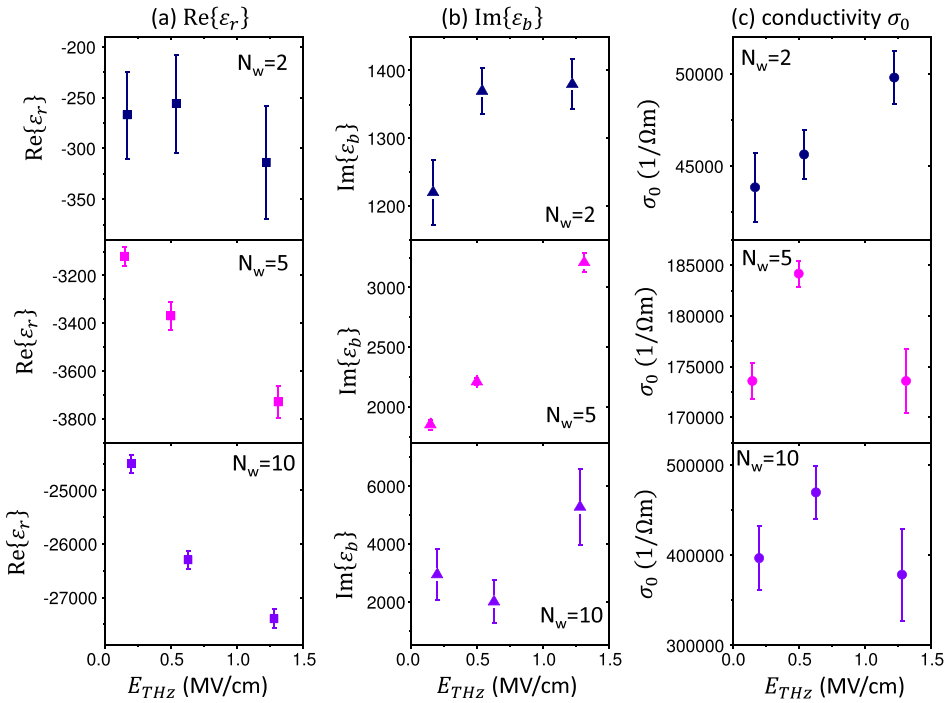

FIG. 5. Dielectric constant and conductivity: (a) Real part of dielectric constant Re(ε_r); (b) imaginary part of ε_b, the contribution from bound electrons; and (c) DC conductivity σ_0 for $N_w = 2$, 5, and 10.

In conclusion, strong THz pulses give rise to highly anisotropic linear and nonlinear responses in free-standing MWNTs. In particular, intense THz fields induce large nonlinear absorption for the polarization parallel to the CNT axis, while no nonlinear response is observed in the perpendicular case. A theoretical analysis based on the Drude model suggests that strong THz fields enhance the permittivity of the MWNTs, inducing strong nonlinear electron dynamics.

The OSU work was supported by the National Science Foundation (DMR-1063632). The SNU work was supported by the National Research Foundation of Korea (NRF) Grant funded by the Korea Government (MSIP: NRF-2015R1A3A2031768).

[1]Z. Zhong, N. M. Gabor, J. E. Sharping, A. L. Gaeta, and P. L. McEuen, Nat. Nanotechnol. **3**, 201 (2008).
[2]M. J. Paul, N. A. Kuhta, J. L. Tomaino, A. D. Jameson, L. P. Maizy, T. Sharf, N. L. Rupesinghe, K. B. K. Teo, S. Inampudi, V. A. Podolskiy, E. D. Minot, and Y.-S. Lee, Appl. Phys. Lett. **101**, 111107 (2012).
[3]M. V. Shuba, A. G. Paddubskaya, A. O. Plyushch, P. P. Kuzhir, G. Y. Slepyan, S. A. Maksimenko, V. K. Ksenevich, P. Buka, D. Seliuta, I. Kasalynas, J. Macutkevic, G. Valusis, C. Thomsen, and A. Lakhtakia, Phys. Rev. B **85**, 165435 (2012).
[4]R. R. Hartmann, J. Kono, and M. E. Portnoi, Nanotechnology **25**, 322001 (2014).
[5]T. Fuse, Y. Kawano, M. Suzuki, Y. Aoyagi, and K. Ishibashi, Appl. Phys. Lett. **90**, 013119 (2007).
[6]D. Kienle and F. Léonard, Phys. Rev. Lett. **103**, 026601 (2009).
[7]A. D. Franklin, M. Luisier, S.-J. Han, G. Tulevski, C. M. Breslin, L. Gignac, M. S. Lundstrom, and W. Haensch, Nano Lett. **12**, 758 (2012).
[8]O. V. Kibis, M. R. Da Costa, and M. E. Portnoi, Nano Lett. **7**, 3414 (2007).
[9]L. V. Titova, C. L. Pint, Q. Zhang, R. H. Hauge, J. Kono, and F. A. Hegmann, Nano Lett. **15**, 3267 (2015).
[10]M. Rinzan, G. Jenkins, H. D. Drew, S. Shafranjuk, and P. Barbara, Nano Lett. **12**, 3097 (2012).
[11]X. He, N. Fujimura, J. M. Lloyd, K. J. Erickson, A. A. Talin, Q. Zhang, W. Gao, Q. Jiang, Y. Kawano, R. H. Hauge, F. Lonard, and J. Kono, Nano Lett. **14**, 3953 (2014).
[12]S.-L. Chen, Y.-C. Chang, C. Zhang, J. G. Ok, T. Ling, M. T. Mihnev, T. B. Norris, and L. J. Guo, Nat. Photonics **8**, 537 (2014).
[13]M. A. Seo, J. H. Yim, Y. H. Ahn, F. Rotermund, D. S. Kim, S. Lee, and H. Lim, Appl. Phys. Lett. **93**, 231905 (2008).
[14]C. J. Docherty, S. D. Stranks, S. N. Habisreutinger, H. J. Joyce, L. M. Herz, R. J. Nicholas, and M. B. Johnston, J. Appl. Phys. **115**, 203108 (2014).
[15]L. Ren, C. L. Pint, L. G. Booshehri, W. D. Rice, X. Wang, D. J. Hilton, K. Takeya, I. Kawayama, M. Tonouchi, R. H. Hauge, and J. Kono, Nano Lett. **9**, 2610 (2009).
[16]J. Kyoung, E. Y. Jang, M. D. Lima, H.-R. Park, R. O. Robles, X. Lepró, Y. H. Kim, R. H. Baughman, and D.-S. Kim, Nano Lett. **11**, 4227 (2011).
[17]L. Ren, C. L. Pint, T. Arikawa, K. Takeya, I. Kawayama, M. Tonouchi, R. H. Hauge, and J. Kono, Nano Lett. **12**, 787 (2012).
[18]S. Watanabe, N. Minami, and R. Shimano, Opt. Express **19**, 1528 (2011).
[19]M. J. Paul, Y. C. Chang, Z. J. Thompson, A. Stickel, J. Wardini, H. Choi, E. D. Minot, B. Hou, J. A. Nees, T. B. Norris, and Y.-S. Lee, New J. Phys. **15**, 085019 (2013).
[20]M. J. Paul, B. Lee, J. L. Wardini, Z. J. Thompson, A. D. Stickel, A. Mousavian, H. Choi, E. D. Minot, and Y.-S. Lee, Appl. Phys. Lett. **105**, 221107 (2014).
[21]M. Zhang, S. Fang, A. A. Zakhidov, S. B. Lee, A. E. Aliev, C. D. Williams, K. R. Atkinson, and R. H. Baughman, Science **309**, 1215 (2005).
[22]A. A. Kuznetsov, A. F. Fonseca, R. H. Baughman, and A. A. Zakhidov, ACS Nano **5**, 985 (2011).
[23]Y.-G. Jeong, M. J. Paul, S.-H. Kim, K.-J. Yee, D.-S. Kim, and Y.-S. Lee, Appl. Phys. Lett. **103**, 171109 (2013).
[24]L. Duvillaret, F. Garet, and J.-L. Coutaz, IEEE J. Sel. Top. Quantum Electron. **2**, 739 (1996).
[25]V. Perebeinos and P. Avouris, Phys. Rev. B **74**, 121410 (2006).
[26]V. Perebeinos and P. Avouris, Nano Lett. **7**, 609 (2007).
[27]N. M. Gabor, Z. Zhong, K. Bosnick, J. Park, and P. L. McEuen, Science **325**, 1367 (2009).